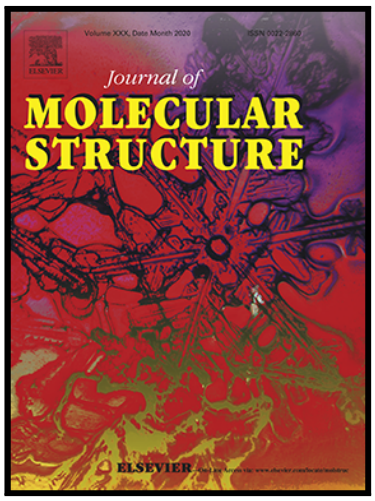

Matrix Isolation of Vapors from 1,2,4-Triazolium Salts: Exploring the Generation of N-Heterocyclic Carbenes

Tatiana Caneca , Epole Ntungwe , Leonardo J. Duarte , A. J. Lopes Jesus , Cláudio M. Nunes , Rui Fausto

PII: S0022-2860(25)01731-4
DOI: https://doi.org/10.1016/j.molstruc.2025.143058
Reference: MOLSTR 143058

To appear in: *Journal of Molecular Structure*

Received date: 28 March 2025
Revised date: 9 May 2025
Accepted date: 20 June 2025

Please cite this article as: Tatiana Caneca , Epole Ntungwe , Leonardo J. Duarte , A. J. Lopes Jesus , Cláudio M. Nunes , Rui Fausto , Matrix Isolation of Vapors from 1,2,4-Triazolium Salts: Exploring the Generation of N-Heterocyclic Carbenes, *Journal of Molecular Structure* (2025), doi: https://doi.org/10.1016/j.molstruc.2025.143058

Highlights

- Vapors from 1,2,4-triazolium salts were condensed in an Ar matrix.
- Spectroscopic analysis reveals NHC formation in the trifluoroacetate salt.
- No NHC is observed in the iodide salt. Triazoles and methyl iodide were identified.
- The distinct behavior of the two salts highlights the role of the counterion basicity.
- DFT calculations and molecular dynamics simulations provided structural insights.

Matrix Isolation of Vapors from 1,2,4-Triazolium Salts: Exploring the Generation of *N*-Heterocyclic Carbenes

Tatiana Caneca,[a] Epole Ntungwe,[a] Leonardo J. Duarte, [a,b] A. J. Lopes Jesus,[c*] Cláudio M. Nunes,[a*] and Rui Fausto [a,d]

[a] *University of Coimbra, CQC-IMS, Department of Chemistry, 3004-535, Coimbra, Portugal.*

[b] *Institute of Chemistry, Department of Fundamental Chemistry, University of São Paulo, 05508-900, São Paulo, Brazil*

[c] *University of Coimbra, CQC-IMS, Faculty of Pharmacy, 3000-548, Coimbra, Portugal.*

[d] *Spectroscopy@IKU, Istanbul Kultur University, Faculty Sciences and Letters, Department of Physics, 34158 Bakirkoy, Istanbul, Turkey*

* Corresponding authors:

A. J. Lopes Jesus, E-mail ajorge@ff.uc.pt

Cláudio M. Nunes, E-mail: cmnunes@qui.uc.pt

Abstract

The generation of the carbenic species 1,4-dimethyl-1,2,4-triazol-5-ylidene **DMTr** was explored via the sublimation of 1,4-dimethyl-1,2,4-triazolium iodide **[DMTrH$^+$][I$^-$]** and the vaporization of 1,4-dimethyl-1,2,4-triazolium trifluoroacetate **[DMTrH$^+$][TFA$^-$]**. Thermal stability of both salts was first assessed by thermogravimetric analysis. Vapors were then generated by heating the samples under vacuum and subsequently trapped in a low-temperature Ar matrix (15 K). In both cases, the matrix-isolation IR spectra differed from those of the pure salts, indicating thermal transformations. The outcomes these transformations varied between the two compounds. For **[DMTrH$^+$][I$^-$]**, no spectral indication of **DMTr** carbene was observed. Instead, 1-methyl- and 4-methyl-1,2,4-triazoles, along with CH_3I, were identified. For **[DMTrH$^+$][TFA$^-$]**, trifluoroacetic acid **HTFA** was detected, suggesting the concurrent formation of **DMTr** carbene. These contrasting outcomes highlight the pivotal influence of the counterion basicity (iodide *vs* trifluoroacetate) in dictating the transformations of the triazolium salt. The less basic iodide attacks one of the methyl groups, leading to C–N bond cleavage and the formation of neutral triazole, whereas the more basic trifluoroacetate promotes proton transfer. Complementary DFT calculations of ion pair interactions and *ab initio* molecular dynamics simulations of the bulk **[DMTrH$^+$][TFA$^-$]** ionic liquid provided further structural insights and helped rationalize the distinct behavior of the two triazolium salts upon trapping their vapors in the cryogenic Ar matrix.

Keywords: 1,2,4-triazolium salts, *N*-heterocyclic carbenes, matrix-isolation, IR spectroscopy, computational chemistry.

1. Introduction

The thiazolium salt coenzyme thiamine **1** (vitamin B1; see Scheme 1) is a natural powerhouse molecule that catalyzes several biochemical processes involving nucleophilic acylation reactions [1,2]. In 1943, Ukai et al. reported the pioneering discovery that thiamine and other thiazolium salts catalyze the benzoin condensation [3]. In a landmark paper in 1958, Breslow proposed the corresponding reaction mechanism, suggesting that a thiazol-2-ylidene **2** (a carbene) is the key catalytically active species, formed *in situ* by base-mediated deprotonation of the thiazolium salt [4] (Scheme 1). Over the past three decades, significant advances in understanding carbene reactivity have contributed to the development of organocatalytic reactions enabled by *N*-heterocyclic carbenes (NHCs) as a cornerstone of modern synthetic methodologies [5–7]. Surface-assisted generation of NHCs has gained increasing attention in recent years. This approach has enabled the covalent immobilization of NHCs onto gold and other metal surfaces, yielding robust and functional interfaces with applications in catalysis, biosensing, and materials science [8–10].

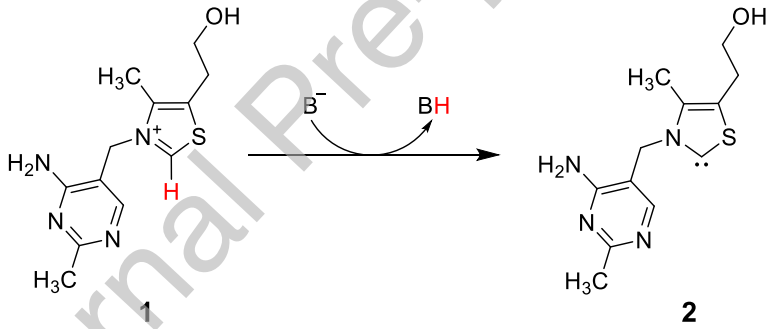

1 **2**

Scheme 1. Molecular structure of thiamine **1** (vitamin B1) and its base-mediated (B^-) deprotonation, leading to the formation of a thiazol-2-ylidene **2** (carbene).

NHCs are typically defined as heterocycles containing a carbene carbon and at least one α-nitrogen atom in the ring structure [11]. Carbenes are neutral species containing a divalent carbon possessing a six-electron valence shell, making them generally unstable and highly reactive [12]. In 1997, Maier et al. generated the simplest thiazol-2-ylidene **4** by photodecarboxylation of thiazole-2-carboxylic acid **3** under matrix isolation conditions (Scheme 2). This approach enabled the IR spectroscopic characterization of the generated carbene, providing valuable insights into its structure and reactivity [13]. Using a similar approach, they also reported the generation of the simplest imidazol-2-ylidene **6** from imidazole-2-carboxylic acid **5** [14] (Scheme 2). With the introduction of two *N*-adamantyl

substituents on imidazol-2-ylidene, in 1991, Arduengo et al. achieved a major breakthrough by synthesizing the first stable NHC [15]. Later, in 1995, Enders, Teles et al. developed the first commercially available NHC derived from a 1,2,4-triazol-5-ylidene framework, which was stabilized by three phenyl-substituted rings, and obtained as a crystalline, isolable compound [16]. The steric effects introduced by the substituents and the electronic contribution provided by the nitrogen atoms significantly enhance the stability of NHCs. As these species adopt a singlet ground state with a sp^2-hybridized carbene carbon, stabilization through σ-electron withdrawing effects (decreasing the energy of the *s*-orbital) and π-electron donating effects (increasing the resonance with the unoccupied *p*-orbital) is also influenced by the nature of substituents attached to the vicinal nitrogen atoms and by the aromaticity of the heterocyclic ring [11,17]. Notably, triazole-derived carbenes have emerged as particularly efficient and promising NHCs in organocatalysis [5,6,18]. Although these NHCs are typically reported to be generated *in situ* by the deprotonation of the corresponding triazolium salt, fundamental studies on their nature remain limited [19–21].

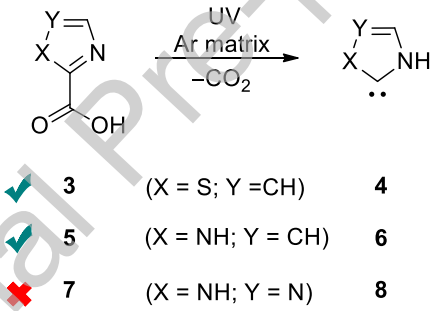

Scheme 2. Photodecarboxylation of thiazole-2-carboxylic acid **3** and imidazole-2-carboxylic acid **5** under matrix isolation conditions (Ar, 10 K), leading to the formation of thiazol-2-ylidene **4** and imidazol-2-ylidene **6**, respectively. Our attempt to generate 1,2,4-triazol-5-ylidene **8** via photodecarboxylation of 1,2,4-triazole-3-carboxylic acid **7** was unsuccessful (see Figure S1).

In this context, we become interested in exploring the generation of simple 1,2,4-triazol-5-ylidenes in cryogenic matrices. Our initial plan aimed to produce the parent 1,2,4-triazol-5-ylidene **8** via photodecarboxylation of 1,2,4-triazole-3-carboxylic acid **7** (Scheme 2), following an approach analogous to that by Maier et al. [13,14]. However, consistently with the results reported by Wierzejewska et al. [22], our attempts were unsuccessful, as sublimation of **7** exclusively led to the isolation of 1,2,4-triazole **9** and CO_2 in an Ar matrix at 15 K (see Figure S1 in the supplementary material for details).

We then turned our attention to exploring the vapors of 1,2,4-triazolium salts as a potential source for generating the corresponding NHCs. In 2015, Sander et al. reported that vapors of 1-ethyl-3-methylimidazolium acetate **[EMImH$^+$][Ac$^-$]** (imidazole salt ionic liquid) were trapped in solid Ar or N_2 as 1-ethyl-3-methylimidazol-2-ylidene **EMIm** and acetic acid **HAc**, with no ionic species detected (Scheme 3) [23]. These findings aligned with the photoelectron spectroscopy, mass spectrometry and computational studies by Nyulaszi el al., which indicated that the gas-phase equilibrium of **[EMImH$^+$][Ac$^-$]** is shifted toward the formation of neutral species via proton transfer, forming either the hydrogen bonded complex **[EMIm]:[HAc]** at moderate low vapor pressures or the free **EMIm** and **HAc** at very low vapor pressures (ca. 10^{-6} mbar) [24]. When vapors of **[EMImH$^+$][Ac$^-$]** were deposited in a film at cryogenic temperatures, the trapped **EMIm** and **HAc** reverted to the salt **[EMImH$^+$][Ac$^-$]** during the warming at room temperature [23] (Scheme 3). Interestingly, the carbene concentration from **[EMImH$^+$][Ac$^-$]** in solution is sufficient to catalyze benzoin condensation and other reactions, revealing the potential of ionic liquids for organocatalysis [25]. In the gas-phase equilibrium of such salts, the tendency to form neutral species seems to depend on the basicity of the ionic components [24]. For instance, when trifluoromethanesulfonate anion, a much weaker base, is used instead of acetate anion, the **[EMImH$^+$][TfO$^-$]** salt (also an ionic liquid) was trapped in as 1:1 cation-anion pair in a Ne matrix (vaporization temperatures were also notably different: 350 K for acetate *vs* 500 K for trifluoromethanesulfonate) [26].

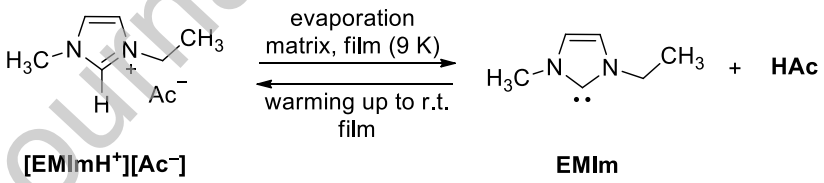

Scheme 3. Formation of carbene **EMIm** and acetic acid **HAc** upon trapping vapors of the ionic liquid **[EMImH$^+$][Ac$^-$]** in Ar and N_2 matrices or in a film (in the absence of a host matrix) at 9 K. The ionic liquid was reformed during the warming of the cryogenic film up to room temperature (r.t.).

To the best of our knowledge, vapors of triazolium salts have not been previously investigated. To address this gap, we report herein a study on the vapors of two triazolium salts (Scheme 4) to assess the feasibility of forming their corresponding carbenes. Our initial focus was on 1,4-dimethyl-4*H*-1,2,4-triazolium iodide **[DMTrH$^+$][I$^-$]**, a widely used NHC precatalyst. However, given that iodide is a very weak base (p$K_a \sim -10$), we extended our study to include the trifluoroacetate derivative **[DMTrH$^+$][TFA$^-$]**, which features a significantly

more basic counterion (pK_a ~ 0.2) [27]. The present investigation integrates experimental and theoretical approaches, including low-temperature matrix isolation infrared spectroscopy, thermal analysis, DFT calculations for the ionic pairs of the studied salts and other putative species that may result from their thermal decomposition, and *Ab* Initio Molecular Dynamics (AIMD) simulations of the bulk **[DMTrH$^+$][TFA$^-$]** ionic liquid.

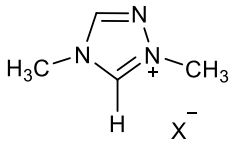

[DMTrH$^+$][X$^-$]

X = I$^-$ or TFA$^-$

Scheme 4. Representation of the 1,2,4-triazolium salts studied in the present work: 1,4-dimethyl-4*H*-1,2,4-triazolium iodide **[DMTrH$^+$][I$^-$]** and 1,4-dimethyl-4*H*-1,2,4-triazolium trifluoroacetate **[DMTrH$^+$][TFA$^-$]**.

2. Materials and methods

2.1. Materials

1,4-Dimethyl-4*H*-1,2,4-triazolium iodide **[DMTrH$^+$][I$^-$]** (Sigma-Aldrich, > 98%) and silver trifluoroacetate (Sigma-Aldrich, 98%) were used as received.

2.2. Synthesis

The synthesis of the ionic liquid 1,4-dimethyl-4*H*-1,2,4-triazolium trifluoroacetate **[DMTrH$^+$][TFA$^-$]** was performed using the adaption of an experimental procedure described elsewhere [28]. Briefly, **[DMTrH$^+$][I$^-$]** (23.46 mg, 0.1043 mmol) was dissolved in anhydrous acetone (4 mL) in a round-bottomed flask. Silver trifluoroacetate (116.27 mg, 0.5264 mmol) was added to this solution and the reaction mixture was stirred overnight at room temperature in the dark. The resulting solid was filtered out, and the solvent was evaporated at room temperature to give a colorless liquid.

Nuclear magnetic resonance (NMR) spectra (^{1}H and ^{13}C) were obtained on a Bruker Avance III spectrometer, operated at 400 MHz at room temperature (Figure S2). The chemical shift values are given in parts per million (ppm) relative to the internal standard (acetone-d6: ^{1}H, 2.05 ppm; ^{13}C, 29.64 ppm). NMR ^{1}H (400 MHz, acetone-d$_6$): δ = 4.13 (3H, s), 4.21 (3H,

s), 9.30 (1H, s), 10.72 (1H, s); NMR ^{13}C (100 M Hz, acetone-d_6): δ = 34.6, 39.1, 118.4 (q, $J_{C\text{-}CF_3}$ = 296), 145.2, 146.4, 160.6 (q, $J_{C\text{-}CF_3}$ = 32).

2.3. Thermal analysis

Thermogravimetric (TGA) and differential scanning calorimetry (DSC) analyses were performed for **[DMTrH$^+$][I$^-$]** and **[DMTrH$^+$][TFA$^-$]** using an SDT Q500 thermal analysis instrument. A few milligrams of the samples were heated from 20 °C to 600 °C at a heating rate of 10 °C min^{-1}, under a nitrogen atmosphere with a flow rate of 20 mL min^{-1}. A Polarized light thermomicroscopy analysis was performed for **[DMTrH$^+$][I$^-$]** upon heating the solid compound from 22 to 135 °C at a scanning rate of 10 °C min^{-1}. A hot stage Linkam system (model DSC600), with a Leica DMRB microscope and a Sony CCD-IRIS/RGB video camera was used. The image analysis was performed using the Real Time Video Measurement System software from Linkam. The images were obtained by combined use of polarized light and wave compensators, using a 200 × amplification.

2.4. Matrix-isolation and IR spectroscopy

In the matrix-isolation experiments, small amounts of **[DMTrH$^+$][I$^-$]** or **[DMTrH$^+$][TFA$^-$]** were placed in a miniature glass oven inside the vacuum chamber of a closed-cycle helium cryostat (APD Cryogenics) equipped with a DE-202A expander. Prior to cooling the cryostat, the samples were pumped at room temperature for several hours at approximately 2 × 10^{-5} mbar to remove traces of water and volatile contaminants. The oven was then heated at ~363 or ~333 K for **[DMTrH$^+$][I$^-$]** or **[DMTrH$^+$][TFA$^-$]**, respectively, using a resistive wire to achieve the vapor pressure necessary for the matrix preparation and the vapors generated from the sublimation or vaporization process were slowly co-deposited with a large excess of Ar onto a cold CsI substrate maintained at 15 K. The temperature was measured directly at the sample holder with an accuracy of 0.1 K, using a silicon diode sensor connected to a digital controller (Scientific Instruments, Model 9650-1). After the deposition, mid-infrared spectra (4000–400 cm^{-1}) of the matrix-isolated compounds were recorded with a resolution of 0.5 cm^{-1}, using a Thermo Nicolet 6700 FTIR spectrometer with a Ge/KBr beam splitter and a deuterated triglycine sulfate (DTGS) detector.

In addition to recording IR spectra under matrix isolation conditions, IR spectra of the pure 1,2,4-triazolium salts were also recorded at room temperature by placing a droplet of the sample onto the diamond crystal of an ATR-FTIR spectrometric system.

2.5. Computational methods

The geometries of the ion pairs of the **[DMTrH$^+$][I$^-$]** and **[DMTrH$^+$][TFA$^-$]** salts were fully optimized using the B3LYP (DFT) functional [29–31]. The 6-311+G(2d,p) basis set [32] was employed for all atoms, with the exception of iodine, which was treated using the LANL2DZ basis set [33]. To account for dispersion interactions and basis set superposition error (BSSE), the Grimme's D3 dispersion correction with Becke-Johnson damping (GD3BJ) [34] and counterpoise correction were applied. For species other than ion pairs, full geometry optimizations were performed without dispersion correction. Harmonic vibrational frequency calculations were carried out on the optimized geometries at the same level of theory. The calculated vibrational frequencies were scaled by a factor of 0.980, accounting for vibrational anharmonicity, basis set limitations, and partial neglect of electron correlation effects. In some cases, IR spectra were simulated with Lorentzian functions with a full width at half-maximum (FWHM) of 2 or 8 cm^{-1}, with the area of each simulated IR band (peak intensities shown in arbitrary units of "relative intensity") corresponding to the calculated IR intensities (in km mol^{-1}). All computations were performed using the Gaussian 16 software package (version B.01) [35].

The computational characterization of the **[DMTrH$^+$][TFA$^-$]** ionic liquid was also performed using molecular dynamics. This was done for this specific case since the high Coulomb interactions between the ions in the bulk of the liquid are not expected to match the most stable dimer structure in gas phase. To calculate the IR spectrum in the bulk liquid phase, we utilized classical Molecular Dynamics (MD) with LAMMPS [36], followed by an *Ab Initio* Molecular Dynamics (AIMD) simulation with CP2K [37]. The simulation cell was constructed with PACKMOL [38] using the optimized structures of **DMTrH$^+$** and **TFA$^-$**, and a reparametrized force field using DFT calculations (the force field can be found in the supplementary material, see computational data). The cell contains 72 molecules: 36 **DMTrH$^+$** and 36 **TFA$^-$**. The classical simulation was performed in three steps: an energy minimization step, followed by an NVT simulation at 300 K and 1 bar with a massive thermostat for 2000 fs. The last step is an NPT simulation for 2500 fs until the cell density becomes stable. The classically equilibrated cell is utilized as the starting point for the AIMD simulation. AIMD

dynamics were conducted at the BLYP/DZVP-MOLOPT-SR-GTH level [39] with the GTH-BLYP-q pseudopotential for the core electrons [40]. The steps for the AIMD simulation are massive equilibration, global equilibration, and production. The massive equilibration was done using an NVT ensemble and a massive Nosé-type thermostat for 2000 fs (2k steps of 1 fs). The global equilibration used an NVT ensemble and a global thermostat for 2500 fs (5k steps of 0.5 fs). The production run also used an NVT ensemble with a global Nosé-type thermostat for 15 ps (30k steps of 0.5 fs). Finally, to compute the IR spectrum in the liquid phase, the TRAVIS software [41] was used following a procedure described elsewhere [39].

3. Results and discussion

3.1. Structure of the ion pairs

The structures of ions pairs of the **[DMTrH$^+$][I$^-$]** and **[DMTrH$^+$][TFA$^-$]** salts, denoted as **[DMTrH$^+$···X$^-$]** (DMTrH$^+$ represents the 1,4-dimethyl-4*H*-1,2,4-triazolium cation and X$^-$ refers to the I$^-$ or TFA$^-$ anion, see Scheme 4), were characterized through DFT(B3LYP) theoretical calculations. The starting geometries were generated by positioning the anions in chemically intuitive locations around the triazolium cation, assuming potential hydrogen bonding, electrostatic interactions, and steric effects, and also guided by computational results reported for similar systems [42,43]. Geometry optimizations, followed by vibrational analyses, were then performed at the B3LYP/6-311+G(2d,p)[LANL2DZ]-GD3BJ or B3LYP/6-311+G(2d,p)-GD3BJ level for the **[DMTrH$^+$···I$^-$]** or **[DMTrH$^+$···TFA$^-$]** ion pairs, respectively, as outlined in the computational methods section.

For the **[DMTrH$^+$···I$^-$]** ion pair, a single minimum energy structure was identified and is depicted in Figure 1. In this structure, the iodide ion is positioned out the triazolium ring plane, in the proximity of the C5−H fragment. The calculated C5−H···I distance of 2.95 Å is close to the sum of the van der Waals radii of hydrogen and iodine (3.08 Å), suggesting a very weak or negligible interaction between the iodide anion and the triazolium ring. This result is consistent with the very low basicity of I$^-$, which limits its ability to form a strong interaction with the C5 H-atom. Regarding the **[DMTrH$^+$···TFA$^-$]** ion pair, five stable structures were identified (see Figure S3), but only two of them were found to be energetically relevant (**I** and **II** in Figure 1; the relative Gibbs free energies computed for all the remaining are higher than 18 kJ mol^{-1}). In both cases, the carboxylate group of the anion establishes two C−H···O hydrogen bonds with the triazolium cation: one with the C5 H-atom (C5−H···O) and the other with a methyl H-atom (C6−H···O in **II** or C7−H···O in **I**). The geometric parameters

characterizing these interactions, included in Figure 1, reveal that the C5−H···O bond is significantly stronger than the C6−H···O or C7−H···O ones. This difference can be attributed to the higher acidity of the C5 H-atom compared to the methyl hydrogens.

The computational results on the structure of the monomeric units described above suggest that experimental access to 1,4-dimethyl-1,2,4-triazol-5-ylidene **DMTr** is more likely to occur via vapors of **[DMTrH$^+$][TFA$^-$]** than **[DMTrH$^+$][I$^-$]**. This preference arises from the presence of a C5−H···O hydrogen-bonding interaction in the former, which is expected to facilitate proton transfer by bringing the anion into close proximity with the acidic proton at C5, thereby promoting the formation of neutral species. Additionally, the significantly higher basicity of TFA$^-$ (pK_a ~ 0.2) compared to I$^-$ (pK_a ~ −10) is likely to play a role in stabilizing the deprotonated form, further favoring the generation of **DMTr**.

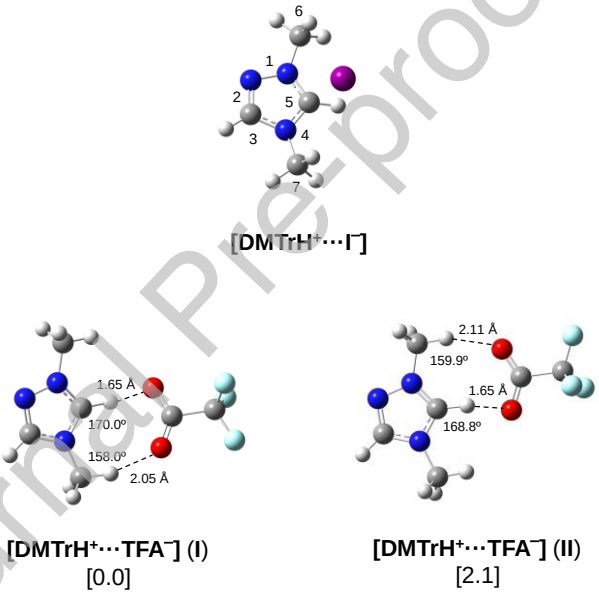

Figure 1. B3LYP/6-311+G(2d,p)[LANL2DZ]-GD3BJ optimized geometry of the **[DMTrH$^+$···I$^-$]** ion pair (atom numbering is given for the 1,2,4-triazolim cation) and B3LYP/6-311+G(2d,p)-GD3BJ optimized geometries of the two most stable minima (labelled as **I** and **II**) of the **[DMTrH$^+$···TFA$^-$]** ion pair (values in square brackets are the relative Gibbs energies at 298.15 K in kJ mol^{-1}). The geometric parameters refer to the H···O distances (Å) and C−H···O angles (º) for the hydrogen bonds formed.

3.2. Thermal stability of the 1,2,4-triazolium salts

Thermogravimetric analysis was performed on the 1,2,4-triazolium salts to evaluate their short-term thermal stability, and the results are presented in Figure S4. Both salts exhibit a slight mass loss in the 50–120 ºC range, which may be attributed to moisture evaporation in

the case of the **[DMTrH$^+$][I$^-$]** solid salt, or to the evaporation of residual solvent from the synthesis process in the case of the **[DMTrH$^+$][TFA$^-$]** liquid salt. For the solid salt, the initial slight mass loss is accompanied by a small endothermic peak at 121ºC in the DSC curve, corresponding to the melting of the compound, as confirmed by polarized light thermomicroscopy analysis (Figure S5). Significant decomposition is observed for the two salts at temperatures above 140–150ºC, as indicated by a marked mass loss. The characteristic decomposition temperatures, determined from the onset of the DTG curves, were found to be 182 ºC for the solid **[DMTrH$^+$][I$^-$]** and 157 ºC for the liquid **[DMTrH$^+$][TFA$^-$]**. These values are comparable to those reported for a series of 1-alkyl-4-methyl-1,2,4-triazolium ionic liquids [24]. However, it is important to note that the actual degradation may begin at a lower temperature than the onset temperature determined in this type of DTG experiments [44]. Indeed, for these 1,2,4-triazolium salts, this scenario is clearly supported by the matrix-isolation IR spectroscopy experiments, as discussed below.

*3.3. IR spectra of solid **[DMTrH$^+$][I$^-$]** and of its vapors trapped in Ar matrix*

[DMTrH$^+$][I$^-$] is commercially available as a powdered compound. In an effort to obtain suitable single crystals for X-ray diffraction analysis, which could provide detailed insights into the crystal structure of the solid salt, several recrystallization attempts were made using various solvents, including acetone, ethyl acetate:hexane, and dichloromethane. Crystals were successfully formed in cooled dichloromethane (~ 6 °C); however, they were found to be fragile and lost their structural integrity when handled at room temperature. A similar issue was encountered with crystals recrystallized from ethyl acetate:hexane under cold conditions, which also lacked stability at ambient temperatures. As a consequence, the experimental ATR IR spectrum of the pure solid salt presented here corresponds to the commercially available powdered form of the compound.

The recorded experimental IR spectrum is shown in Figure 2a in the 1700−500 cm^{-1} range. As observed, it shows a satisfactory agreement with the B3LYP calculated spectrum (Figure 2b) for the **[DMTrH$^+$···I$^-$]** ion pair (Figure 1). From the comparison between the experimental and theoretical spectra, an approximated assignment of the observed bands to specific vibration modes was performed, as detailed in Table S1. The most prominent features in the experimental spectrum appear at 1583, 1166, and 605 cm^{-1}, with the corresponding computed absorptions predicted at 1561, 1163, and 572 cm^{-1}, respectively. The first band is

attributed to ring CN stretching (νCN), the second to ring CH in-plane deformation (δCH), and the third to out-of-plane ring deformations (γC and γN).

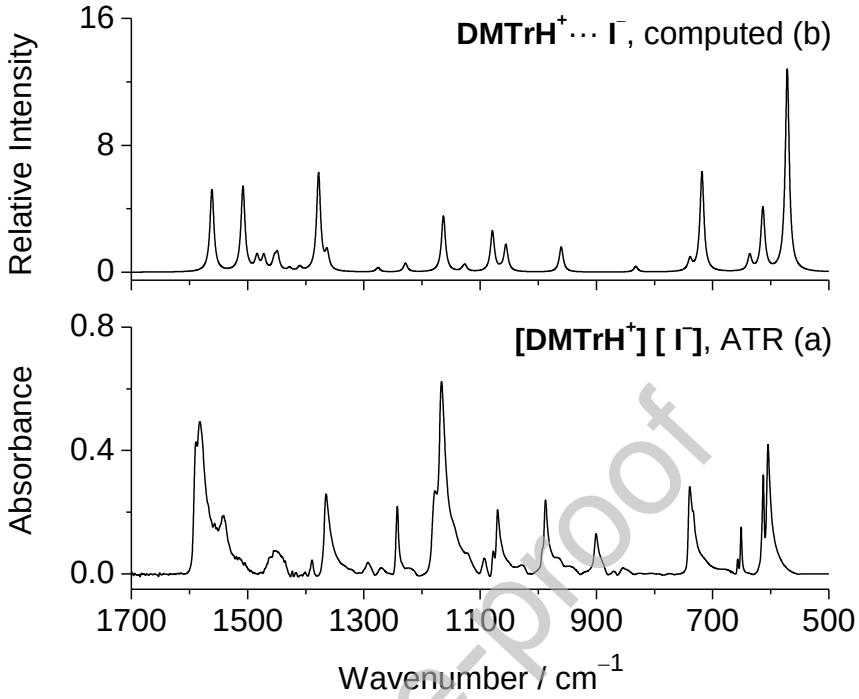

Figure 2. (a) Experimental ATR IR spectrum of **[DMTrH$^+$][I$^-$]** at room temperature. (b) B3LYP/6-311+G(2d,p)[LANL2DZ]-GD3BJ computed IR spectrum of the **[DMTrH$^+$···I$^-$]** ion pair.

Vapors of **[DMTrH$^+$][I$^-$]** were then spectroscopically analyzed using the low-temperature matrix isolation technique. A miniature glass oven, placed inside the vacuum chamber of the cryostat (~10^{-6} mbar), was used to sublime the solid salt at ~363 K. Over the course of a few hours under these conditions, the vapors were gradually co-condensed with a large excess of Ar onto a CsI window at 15 K. The resulting matrix IR spectrum (Figure 3a) showed notable differences compared to the IR spectrum of the solid salt. This dissimilarity clearly excludes the presence of the **[DMTrH$^+$···I$^-$]** ion pair in the low-pressure condensed vapors, meaning that the compound undergoes thermal decomposition. The possible generation of 1,4-dimethyl-1,2,4-triazol-5-ylidene **DMTr** (carbene) and hydrogen iodide **HI**, neutral species resulting from the proton transfer from the triazolium cation to iodide anion, was first analyzed. However, the lack of agreement between the experimental and computed IR spectra of **DMTr** (see Figure S6), along with the absence of any band in the 2237−2254 cm^{-1} range, where monomeric HI trapped in solid Ar is expected to absorb [45], indicates that these species were not formed during the sublimation of the compound.

When searching for other neutral candidates, it was found that the species trapped in the matrix were 1-methyl-1*H*-1,2,4-triazole **10** and 4-methyl-4*H*-1,2,4-triazole **11**, together with methyl iodide **12** (Scheme 5). Most of the bands in the experimental IR spectrum (marked with closed blue circles) are in excellent agreement with the vibrations predicted for **10**, indicating that this should be the major species deposited in the Ar matrix (Figure 3). For instance, the most intense experimental IR bands observed at 1508, 1140, and 679 cm^{-1}, are nicely reproduced by the most intense computed IR bands of **10** at 1509 [ν(CN); δ(CH)], 1140 [ν(CN)], and 681 [γ(C); γ(N)] cm^{-1}. A detailed assignment of the IR spectrum of **10** is given in Table 2. Five of the experimental IR bands that were not attributed to **10** (marked with open red circles) correspond well with the most intense vibrations predicted for **11**, indicating that this species is also present in the argon matrix but in minor amounts. Its most prominent spectral feature is found at 1528 cm^{-1}, with the calculated counterpart predicted at 1521 [ν(CN); δ(CH)]. In addition to the IR bands assigned to the methyl-substituted triazoles **10** and **11**, some of the remaining IR bands observed at 1432, 1400, and 1245 and 528 cm^{-1} (marked with gray squares in Figure 3a) clearly identify the presence of methyl iodide **12**, as evidenced by the perfect match with the most intense bands reported at 1432, 1400, and 1245 and 528 cm^{-1} for an authentic sample of **12** isolated in an Ar matrix [46,47] (see Table 2 for more details).

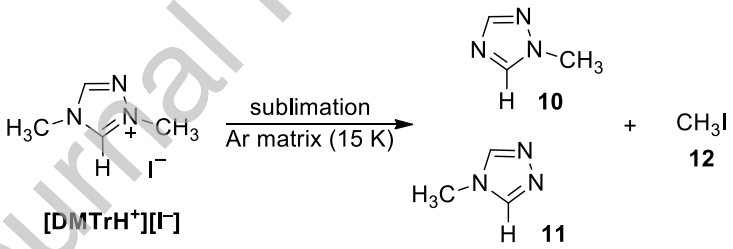

Scheme 5. Thermal decomposition of **[DMTrH$^+$][I$^-$]** during its sublimation (~363 K) and subsequent isolation of the vapors in an Ar matrix at 15 K, which leads to the formation of 1-methyl-1*H*-triazole **10**, 4-methyl-4*H*-triazole **11**, and CH_3I **12**.

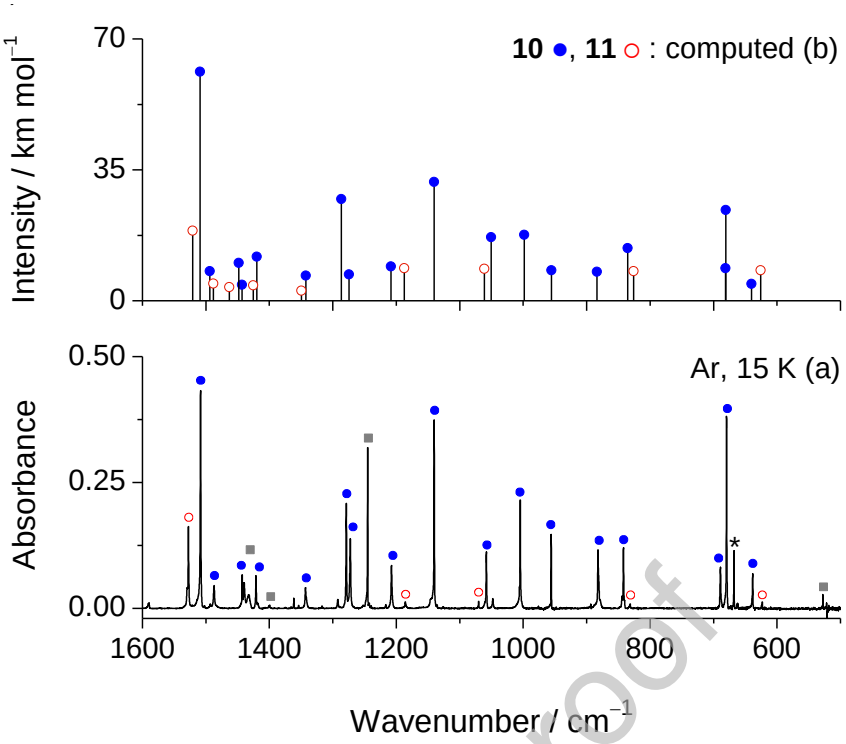

Figure 3. (a) Experimental IR spectrum of the vapors of **[DMTrH$^+$][I$^-$]** trapped in an Ar matrix at 15 K. Bands marked with closed blue circles and open red circles are assigned to **10** and **11**, respectively, based on comparison with their corresponding computed spectra. Bands assigned to methyl iodide **12** are marked with grey squares, with their identification based on the IR spectrum of the compound isolated in an Ar matrix [46]. The band at 668 cm^{-1}, marked with an asterisk (*), is due to atmospheric CO_2. (b) B3LYP/6-311+G(2d,p) computed IR spectrum of 1-methyl-1*H*-1,2,4-triazole **10** (closed blue circles) and 4-methyl-4*H*-1,2,4-triazole **11** (open red circles). The IR intensities of **11** were scaled by 0.3 to provide a **10**:**11** ratio of 1:0.3 that better reproduces the experimental data. Only bands with computed IR intensities > 2 km mol^{-1} are shown.

Table 2. Experimental IR spectrum of vapors of 1,4-dimethyl-4*H*-1,2,4-triazolium iodide **[DMTrH$^+$][I$^-$]** trapped in an Ar matrix at 15 K, B3LYP/6-311+G(2d,p) computed vibrational frequencies ($\tilde{\nu}$, cm^{-1}) and absolute intensities (A^{th}, km mol^{-1}), and vibrational assignment of 1-methyl-1*H*-1,2,4-triazole **10** and 4-methyl-4*H*-1,2,4-triazole **11**. The vibrational assignment of methyl iodide **12** was supported by the reported IR spectrum of authentic sample isolated in Ar matrix.

Exp. (Ar, 15 K) [a]		Calc.		Description [d]
$\tilde{\nu}$	Int.	$\tilde{\nu}$ [c]	A^{th}	
10				
1508	s	1509.0	61.2	$\nu C_5N_4 - \nu C_3N_2$; $\delta C_3H + \delta C_5H$
1487	w	1494.0	7.9	δCH_3 as
1443	w	1448.4	10.1	δCH_3 as'
1440	w	1442.8	4.3	$\nu C_5N_1 - \nu C_3N_2$; δCH_3 s
1421	w	1419.7	11.7	δCH_3 s; $\nu C_5N_1 - \nu C_6N_1$
1343	w	1342.6	6.7	$\nu C_5N_4 + \nu C_3N_2$
1279	m	1286.7	27.2	$\nu C_3N_2 + \nu C_3N_4 - \nu C_5N_4$
1272	m	1274.1	7.1	νN_1N_2; $\delta N_1C_5N_4$
1208	w	1208.3	9.1	$\delta C_3H - \delta C_5H$
1140	s	1140.1	31.7	$\nu C_3N_4 + \nu C_5N_4$
1058	m	1050.4	17.0	ρCH_3
1005	m	998.3	17.6	νN_1N_2; $\delta N_1N_2C_3$
956	m	955.3	8.1	$\delta C_3N_4C_5$
882	m	883.9	7.7	γC_3; γC_3H
842	m	835.1	14.1	γC_5; γC_5H
689	w	681.0	8.7	νC_6N_1; $\delta C_5N_1N_2$
679	s	680.7	24.2	$\gamma C_3 - \gamma N_2 - \gamma N_4$
639	w	640.3	4.5	$\gamma C_5 - \gamma N_1 + \gamma N_2$
11				
1528	m	1521.0	62.3	$\nu C_3N_2 - \nu C_5N_1$; $\delta C_3H + \delta C_5H$
1186	w	1187.3	28.9	νC_6N_4; $\delta C_3H + \delta C_5H$
1070	w	1061.2	28.4	$\nu C_5N_4 + \delta C_3N_4$; $\delta C_3N_4C_5$
831	w	825.8	26.3	$\gamma C_3 + \gamma C_5$; $\gamma C_3H + \gamma C_5H$
623	w	625.9	27.2	$\gamma C_3 + \gamma C_5 - \gamma N_4$
12 [b]				
1432 (1432)	w	1443.5	5.5	δCH_3 as
1400 (1400)	w	–	–	[e]
1245 (1245)	s	1261.0	33.2	δCH_3 s
n.o. (880)	–	882.9	8.6	ρCH_3
528 (528)	–	499.7	4.6	νCI

[a] IR absorptions in the high frequency region, corresponding to CH and CH_3 stretching vibrations, were not analyzed. Abbreviations: n.o. = not observed due to overlap with the band of **11** at 882 cm^{-1}. Experimental wavenumbers are given in cm^{-1} while the intensities (Int.) are expressed qualitatively: s = strong; m = medium; w = weak. [b] Wavenumbers in brackets correspond to the IR bands observed for an authentic sample of CH_3I isolated in solid Ar and were taken from Ref. [46]. [c]Calculated harmonic wavenumbers were multiplied by 0.980. [d] Abbreviations: ν, stretching; δ, in-plane bending; ρ, rocking; γ, out-of-plane deformation. Signs "+" and "–" designate combination of vibrations occurring in the same phase and in the opposite phase, respectively. [e] Combination band ($\nu CI + \rho CH_3$), see Ref. [46].

In summary, the spectroscopic results demonstrate that upon sublimation of **[DMTrH$^+$][I$^-$]**, the formation of **DMTr** carbene via abstraction of the H-atom at C5 by iodide ion does not occur. This appears to be due to the very low basicity of iodide, which does not favor the deprotonation reaction at C5 (consistent also with the computed structure of the ion pair presented in section 3.1). Instead, the species identified in the deposited Ar matrix were 1-methyl-1*H*-1,2,4-triazole **10** as the major product, 4-methyl-4*H*-1,2,4-triazole **11** as a minor product, and CH_3I **12** (Scheme 5). These findings clearly show that the thermal decomposition of **[DMTrH$^+$][I$^-$]** proceeds *via* a reverse Menshutkin reaction (reaction of the halide anion with the quaternary ammonium cation leading to the formation of an alkyl halide and tertiary amine). A similar type of thermal decomposition has been reported for some imidazolium halide salts [44,48]. In the triazolium halide salt **[DMTrH$^+$][I$^-$]**, the iodide attacks one of the methyl groups (preferentially that at N1), leading to C–N bond cleavage and the formation of neutral triazole derivatives (preferentially 1-methyl-1*H*-1,2,4-triazole **10**), along with CH_3I.

The predominance of species **10** over species **11** in the deposited Ar matrix is consistent with the computed Gibbs free energy variations for the two reaction pathways outlined in Scheme 5. These values were obtained from calculations performed on the **[DMTrH$^+$··· I$^-$]** ion pair (including counterpoise correction) as well as species **10**, **11**, and **12**. The results indicate that the decomposition pathway leading to the formation of **10** and **12** from the ion pair is significantly more exergonic ($\Delta G \approx -53$ kJ mol^{-1}) compared to the alternative route leading to the formation of **11** and **12** ($\Delta G \approx -18$ kJ mol^{-1}). This pronounced energetic preference for the former pathway is consistent with the well-established greater stability of the 1*H*-tautomeric form of 1,2,4-triazole compared to its 4*H*-tautomeric counterpart [49].

*3.4. IR spectra of liquid **[DMTrH$^+$][TFA$^-$]** and of its vapors trapped in Ar matrix*

The IR spectrum of the synthesized ionic liquid **[DMTrH$^+$][TFA$^-$]**, recorded in ATR mode, is presented in Figure 4a. Upon comparison with the B3LYP computed IR spectrum for the **[DMTrH$^+$···TFA$^-$]** ion pair (structure **I** in Figure 1), a notable difference is observed: the most intense band, computed at ~2500 cm^{-1} and assigned to the stretching vibration of the C5−H bond (*ν*C5H), is absent in the experimental spectrum (Figure 4b). A similar band was predicted for the spectrum of structure **II**. This discrepancy suggests that the most stable ion pair structures of this salt in gas phase may not accurately represent the structure in the liquid phase.

To support this hypothesis, we performed AIMD to simulate the IR spectrum of the bulk ionic liquid. Noteworthy, the computed IR spectrum of the **[DMTrH$^+$][TFA$^-$]** liquid (Figure 4c) does not show any absorption band at ~2500 cm^{-1} and reasonably reproduces the experimental data. Analysis of the radial distribution function between the cation **DMTrH$^+$** and anion **TFA$^-$** indicates a coordination number of 6 (i.e., there are on average six **TFA$^-$** around each unit of **DMTrH$^+$)** (Figure S7). The first coordination sphere extends to a radius of about 4.2 Å, which is significantly larger than the 1.6 Å C5−H···O hydrogen bond length computed for the gas-phase structure (Figure 1). This result is expected since the Coulomb interactions between the ions provide sufficient stabilization to compensate for the missing hydrogen bond interaction. A snapshot of the simulation trajectory, showing the interaction between the **DMTrH$^+$** and **TFA$^-$** ions, is compared with the gas-phase H-bonded structure **I** in Figure 5. Overall, contrary to solid **[DMTrH$^+$][I$^-$]** where IR data suggests that its structure is reasonably described by the most stable ion pairs in the gas phase, liquid **[DMTrH$^+$][TFA$^-$]** exhibits a markedly different behavior. The IR data and AIMD simulations reveal that the ions arrangement differs from the most stable gas-phase configuration. This deviation results from an energy gain achieved by increasing the coordination number which disrupts the hydrogen-bonded structure existing in the gas phase ion pairs.

Following the same procedure described for **[DMTrH$^+$][I$^-$]**, vapors of **[DMTrH$^+$][TFA$^-$]** were trapped in an Ar matrix and investigated by matrix-isolation IR spectroscopy. It was observed that the vapors of this 1,2,4-triazolium salt began to emerge at ~333 K. Yet, even a slight increase of temperature resulted in sample decomposition, as evidenced by the appearance of a strong signals at 2349 and 662 cm^{-1} corresponding to the isolation of CO_2 [50]. To minimize such decomposition, trace amounts of the generated vapors at ~333 K were slowly trapped over several hours in an Ar matrix. Nonetheless, as the matrix thickness increased due to the accumulation of host gas on the cryostat optical window, light dispersion in the IR spectrometer also increased, imposing a practical limit on the experiment duration. In our best attempt, matrix-isolation IR spectra were obtained with some bands showing significant absorption and no appreciable amounts of CO_2.

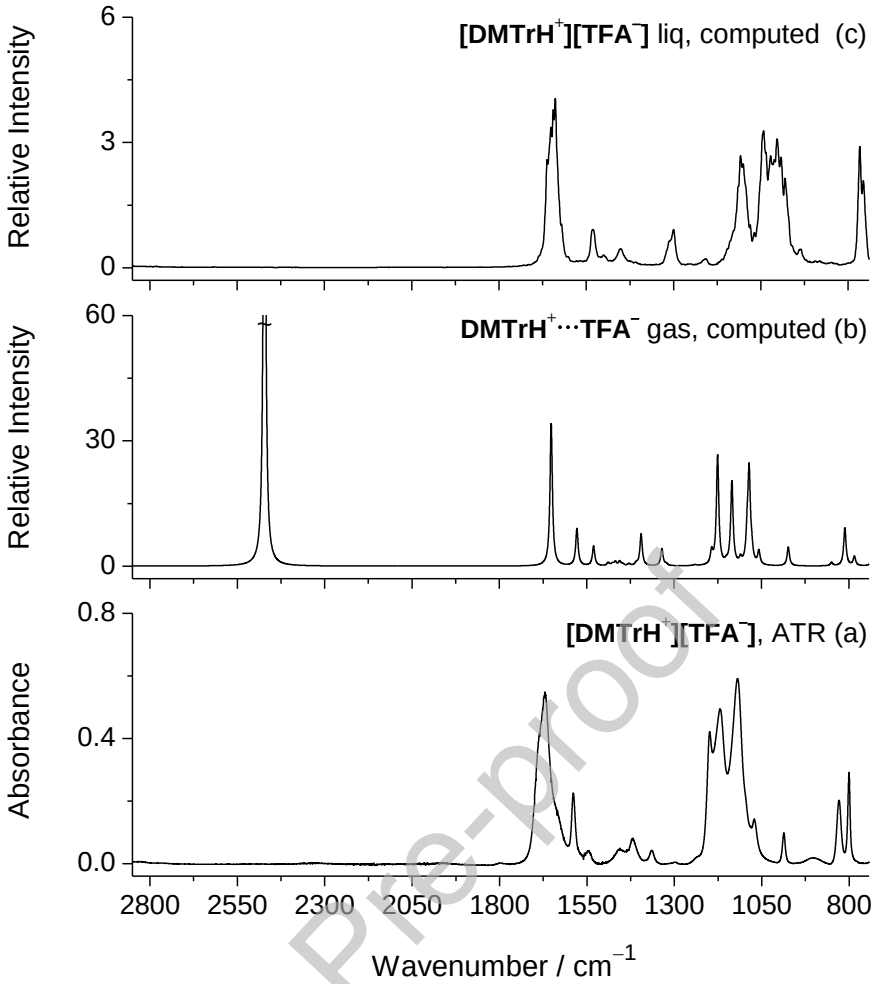

Figure 4. (a) Experimental IR spectrum (ATR) of **[DMTrH⁺][TFA⁻]** as pure liquid at room temperature. (b) B3LYP/6-311+G(2d,p)-GD3BJ computed IR spectrum of the most stable **[DMTrH⁺···TFA⁻]** ion pair (**I**). (c) Theoretical IR spectrum of the **[DMTrH⁺][TFA⁻]** ionic liquid obtained from AIMD simulations.

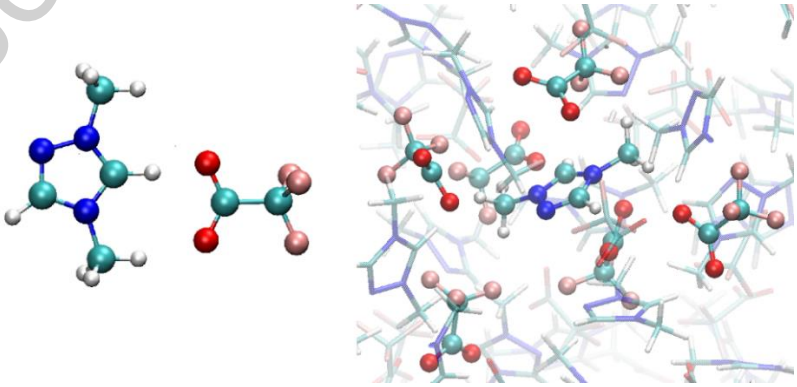

Figure 5. Left: Computed structure of most stable **[DMTrH⁺···TFA⁻]** ion pair (**I**) in gas-phase. Right: Snapshot of the Molecular Dynamics simulation trajectory computed for the bulk liquid **[DMTrH⁺][TFA⁻]**.

Through a simple comparison, it becomes evident that the matrix-isolated IR spectrum do not resemble the IR spectrum for the ionic liquid of **[DMTrH$^+$][TFA$^-$]** nor the computed IR spectrum of the most stable **[DMTrH$^+$···TFA$^-$]** ion pair. Actually, as shown in Figure 6, some of the IR bands were identified as belonging to trifluoroacetic acid **HTFA** isolated in Ar matrix [51]. For instance, the experimental IR bands observed at 3553 [ν(O−H)], 1819 [ν(C=O)], 1250 [ν(CF_3 as'); δ(COH)], 1207 [ν(CF_3 as'); δ(COH); ν(CF_3 s.)], 1204 (not assigned), 1187 [ν(CF_3 as''); δ(CF_3 as'')], 1132/1128 [ν(CO); ν(CF_3) s, δ(COH), δ(CF_3) s] and 1116 (not assigned) cm^{-1}, exactly match the most significant IR absorption reported for an authentic sample of **HTFA** deposited in Ar matrix (assignments taken from ref. [51]).

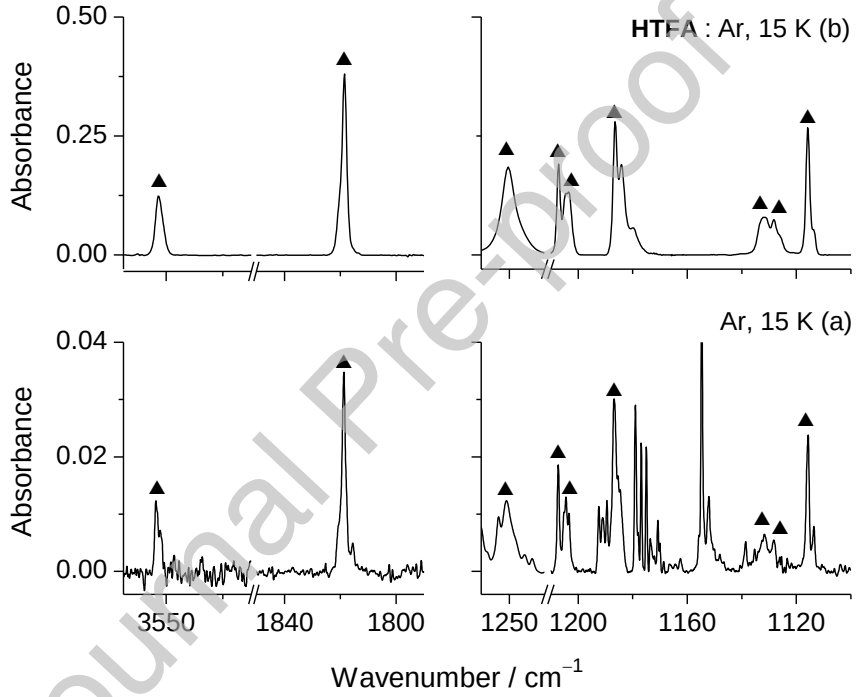

Figure 6. (a) Selected regions of the experimental IR spectrum of the vapors of **[DMTrH$^+$][TFA$^-$]** trapped in an Ar matrix at 15 K. Triangles indicate IR bands assigned to trifluoroacetic acid **HTFA**. (b) Selected regions of the experimental IR spectrum of an authentic sample of **HTFA** deposited in an Ar matrix at 15 K [51].

The identification of **HTFA** from the deposition of vapors of **[DMTrH$^+$][TFA$^-$]** indicates the occurrence of proton transfer from the 1,2,4-triazolium cation **DMTrH$^+$** to the **TFA$^-$** anion. The spectroscopic identification of **HTFA** implies that the corresponding N-heterocyclic carbene, 1,4-dimethyl-1,2,4-triazol-5-ylidene (**DMTr**), should also be present and detectable (Scheme 6). However, when analyzing the computed IR spectrum of **DMTr**, a significant difference in band intensities is observed compared to that of **HTFA** (Figure S8).

The strongest bands in the computed IR spectra of **HTFA** exhibit intrinsic intensities of 300–350 km mol^{-1}, whereas the strongest bands in the **DMTr** spectrum do not exceed 55 km mol^{-1} (the second strongest band in the 2000–400 cm^{-1} region do not exceed 35 km mol^{-1}). This disparity in band intensities could explain the failure to identify the carbene in the matrix, as the lower intensity of the carbene's characteristic bands makes it harder to detect under the experimental conditions.

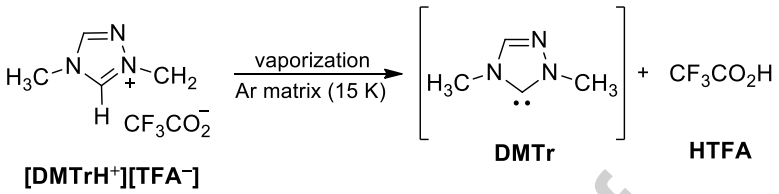

Scheme 6. Thermal decomposition of **[DMTrH$^+$][TFA$^-$]** during vaporization (~333 K) and subsequent isolation of vapors in an Ar matrix at 15 K, which leads to the formation of carbene **DMTr** (not identified) and **HTFA.**

In summary, the results demonstrate that upon sublimation of **[DMTrH$^+$][TFA$^-$]**, the trifluoroacetate ion **TFA$^-$** abstracts the H-atom at C5 forming trifluoroacetic acid **HTFA** and triazole carbene **DMTr**. Due to the very limited amount of vapor that could be produced without decomposition, matrix-isolation IR spectroscopic characterization of **DMTr** was not achieved. The significant basicity of **TFA$^-$** compared to **I$^-$** appears to be key to enabling the proton transfer from the triazolium cation **DMTrH$^+$** and generation of the corresponding conjugated acid **HX** (X = **TFA$^-$**) and triazole carbene **DMTr**. This interpretation is supported by the NMR data presented in Figure S2, where the C5–H proton appears at 10.72 ppm for the trifluoroacetate salt and at 10.57 ppm for the iodide salt. The observed downfield shift confirms a stronger interaction between the more basic TFA$^-$ anion and the C5–H proton, enhancing its acidity and favoring deprotonation.

It shall be notice that experimental results are not easy to interpret straightforwardly. As discussed in Section 3.1, the most stable structure of the **[DMTrH$^+$···TFA$^-$]** ion pair (structure **I** in Figure 1) exhibits a strong C5−H···O hydrogen bond. The B3LYP/6-311+G(2d,p)-GD3BJ computed electronic energy change for the proton transfer between the **DMTrH$^+$** and **TFA$^-$** species, yielding free **DMTr** and **TFA**, was computed to be 25 kcal mol^{-1} (~100 kJ mol^{-1}). A comparable energy change was estimated at the B3LYP/6-31+G* level for the dissociation of the 1-ethyl-3-methylimidazolium acetate **[EMImH$^+$···Ac$^-$]** ion pair into the corresponding imidazole carbene **EMIm** and acetic acid **HAc** (~18 kcal mol^{-1}) [24]. In that system, the

hydrogen bonded complex **[EMIm]:[HAc]** was found to be a minimum with an energy similar to that of the **[EMImH$^+$···Ac$^-$]** ion pair, suggesting that both species exist in a gas-phase equilibrium. The exclusive observation of free **EMIm** and **HAc** in the low-pressure and high-temperature vapors was attributed to a putative entropically favored dissociation process of the thermodynamically more stable complex [23,24]. Our computations show that a hydrogen-bonded complex **[DMTr]:[HTFA]** appear in a shallow potential surface region, ~4 kcal mol^{-1} above the **[DMTrH$^+$···TFA$^-$]** ion pair (Figure S9). Furthermore, the dissociation of the [**DMTrH$^+$···TFA$^-$**] ion pair into free **DMTr** and **TFA** is more endothermic by ~ 7 kcal mol^{-1} compared to the **[EMImH$^+$···Ac$^-$]** ion pair. This can justify the greater difficulty in obtaining the free triazole carbene in the very low-pressure vapors.

Further increasing the basicity of the anions in the triazoles salts should favor the gas-phase equilibrium toward the hydrogen-bonded complex **[DMTr]:[HX]**, facilitating the formation of the carbene **DMTr** at very low pressures. So far, our attempts to prepare 1,4-dimethyl-4*H*-1,2,4-triazolium acetate **[DMTrH$^+$][Ac$^-$]** have failed, which might indicate that the basicity of this anion is too strong (pK_a ~ 4.8 *vs* pK_a ~ 0.2 for trifluoroacetate). Further studies are underway to prepare 1,4-dimethyl-4*H*-1,2,4-triazolium salts with anions more basic than trifluoracetate anion, aiming to enhance the generation of triazole carbenes from their vapor at very low pressures.

4. Conclusions

In this study, the possible generation of the 1,4-dimethyl-1,2,4-triazol-5-ylidene carbenic species (**DMTr**) from 1,2,4-triazolium salts was studied. The approach involved depositing vapors from sublimation/vaporization of selected triazolium salt precursors — specifically, 1,4-dimethyl-1,2,4-triazolium iodide (**[DMTrH$^+$][I$^-$]**) and 1,4-dimethyl-1,2,4-triazolium trifluoroacetate (**[DMTrH$^+$][TFA$^-$]**) — into a cryogenic argon matrix (15 K), followed by infrared spectroscopy analysis supported by theoretical calculations at various levels of theory.

Notably, the two salts exhibited contrasting behaviors: in the case of **[DMTrH$^+$][I$^-$]**, the DMTr carbene was not formed, and 1-methyl- and 4-methyl-1,2,4-triazoles, along with CH_3I, were identified spectroscopically; on the other hand, for **[DMTrH$^+$][TFA$^-$]**, trifluoroacetic acid was detected in the as-deposited matrix, implying concurrent **DMTr** carbene formation, though its weak IR absorption precluded its direct detection. This contrasting behavior of the two studied salts underscores the crucial role of counterion basicity in determining the decomposition pathways: the less basic iodide favours methylation and C–N bond cleavage,

yielding neutral triazoles (1-methyl-1*H*-1,2,4-triazole and 4-methyl-4*H*-1,2,4-triazole, the first corresponding to the favored product, in agreement with its greater stability), while the more basic trifluoroacetate promotes proton transfer.

Complementary DFT calculations of ion pair interactions in both salts, and *ab initio* molecular dynamics simulations of the **[DMTrH$^+$][TFA$^-$]** ionic liquid bulk provided further structural insights, corroborating the experimental observations.

This study offers new insights into the proton transfer dynamics and decomposition behavior of 1,2,4-triazolium salts, highlighting the significance of counterion basicity in carbene generation. Future research will explore triazolium salts with anions of intermediate basicity to optimize carbene formation and characterization. Overall, the findings provide valuable perspectives on the structural and thermochemical factors influencing the stability and reactivity of 1,2,4-triazolium-based ionic species, enhancing our understanding of triazolium-based ionic liquids and their potential applications in catalysis and related fields, and informing the design of thermally stable and reactive ionic compounds for various applications.

CRediT authorship contribution statement: Tatiana I. C. Caneca: investigation. **Epole Ntungwe:** investigation. **Leonardo J. Duarte:** MD calculations and formal analysis. **A. J. Lopes Jesus:** formal analysis, writing – original draft preparation**,** writing–review and editing. **Cláudio M. Nunes:** conceptualization, methodology, writing–review and editing. **Rui Fausto:** resources, project administration, writing–review and editing.

Funding: This work was supported by Project PTDC/QUI-QFI/1880/2020, funded by National Funds via the Portuguese Foundation for Science and Technology (FCT). The Coimbra Chemistry Centre – Institute of Molecular Sciences (CQC-IMS) is supported by FCT through projects UIDB/00313/2020 and UIDP/00313/2020 co-funded by COMPETE and the IMS special complementary funds provided by FCT. The authors acknowledge FCT Advanced Computing Project 2023.10449.CPCA and the Laboratory for Advanced Computing at University of Coimbra (UC-LCA) for providing computing resources that have contributed to the research results reported within this paper and Coimbra Laser Lab (CLL) for experimental facilities. R.F. also acknowledges support from the European Union through the Horizon-Widera-2023-Talents-01 ERA-Chair 1011848998: Spectroscopy@IKU "*Manipulating and Characterizing Molecular Architectures: From Isolated Molecules to Molecular Crystals*".

Acknowledgments:

José A. Paixão and Mário T. S. Rosado are acknowledged for the thermal analysis measurements.

References

[1] S. Chakraborty, A.T. Biju, Birth of organocatalysis by N-heterocyclic carbenes, Nature Catalysis 7 (2024) 1060–1062. https://doi.org/10.1038/s41929-024-01235-z.

[2] M. Pohl, A new perspective on thiamine catalysis, Current Opinion in Biotechnology 15 (2004) 335–342. https://doi.org/10.1016/j.copbio.2004.06.002.

[3] T. Ugai, T. Tanaka, S. Dokawa, A New Catalyst for the Acyloin Condensation., J. Pharm. Soc. Jpn. 63 (1943) 296–300. https://doi.org/10.1248/yakushi1881.63.6_296.

[4] R. Breslow, On the Mechanism of Thiamine Action. IV.1 Evidence from Studies on Model Systems, J. Am. Chem. Soc. 80 (1958) 3719–3726. https://doi.org/10.1021/ja01547a064.

[5] D. Enders, O. Niemeier, A. Henseler, Organocatalysis by N-Heterocyclic Carbenes, Chem. Rev. 107 (2007) 5606–5655. https://doi.org/10.1021/cr068372z.

[6] D.M. Flanigan, F. Romanov-Michailidis, N.A. White, T. Rovis, Organocatalytic Reactions Enabled by N-Heterocyclic Carbenes, Chem. Rev. 115 (2015) 9307–9387. https://doi.org/10.1021/acs.chemrev.5b00060.

[7] X. Chen, H. Wang, Z. Jin, Y.R. Chi, N-Heterocyclic Carbene Organocatalysis: Activation Modes and Typical Reactive Intermediates, Chinese Journal of Chemistry 38 (2020) 1167–1202. https://doi.org/10.1002/cjoc.202000107.

[8] A. Chandran, N.L. Dominique, G. Kaur, V. Clark, P. Nalaoh, L.C. Ekowo, I.M. Jensen, M.D. Aloisio, C.M. Crudden, N. Arroyo-Currás, D.M. Jenkins, J.P. Camden, Forming N-heterocyclic carbene monolayers: not all deposition methods are the same, Nanoscale 17 (2025) 5413–5428. https://doi.org/10.1039/D4NR04428B.

[9] G. Kaur, R.L. Thimes, J.P. Camden, D.M. Jenkins, Fundamentals and applications of N-heterocyclic carbene functionalized gold surfaces and nanoparticles, Chem. Commun. 58 (2022) 13188–13197. https://doi.org/10.1039/D2CC05183D.

[10] Y. Pan, A. Das, F. Glorius, J. Ren, Insights into the surface chemistry of N-heterocyclic carbenes, Chem. Soc. Rev. (2025) 10.1039.D4CS01299B. https://doi.org/10.1039/D4CS01299B.

[11] M.N. Hopkinson, C. Richter, M. Schedler, F. Glorius, An overview of N-heterocyclic carbenes, Nature 510 (2014) 485–496. https://doi.org/10.1038/nature13384.

[12] M. Jones Jr., R.A. Moss, Singlet Carbenes, in: Reactive Intermediate Chemistry, 2003: pp. 273–328. https://doi.org/10.1002/0471721492.ch7.

[13] G. Maier, J. Endres, H.P. Reisenauer, 2,3-Dihydrothiazol-2-ylidene, Angew. Chem. Int. Ed. Engl. 36 (1997) 1709–1712. https://doi.org/10.1002/anie.199717091.

[14] G. Maier, J. Endres, 2,3-Dihydroimidazol-2-ylidene, Eur. J. Org. Chem. 1998 (1998) 1517–1520. https://doi.org/10.1002/(SICI)1099-0690(199808)1998:8<1517::AID-EJOC1517>3.0.CO;2-H.

[15] A.J. Arduengo, R.L. Harlow, M. Kline, A stable crystalline carbene, J. Am. Chem. Soc. 113 (1991) 361–363. https://doi.org/10.1021/ja00001a054.

[16] D. Enders, K. Breuer, G. Raabe, J. Runsink, J.H. Teles, J. Melder, K. Ebel, S. Brode, Preparation, Structure, and Reactivity of 1,3,4-Triphenyl-4,5-dihydro-1 *H* -1,2,4-triazol-5-ylidene, a New Stable Carbene, Angew. Chem. Int. Ed. Engl. 34 (1995) 1021–1023. https://doi.org/10.1002/anie.199510211.

[17] G. Bertrand, Stable Singlet Carbenes, in: Reactive Intermediate Chemistry, 2003: pp. 329–373. https://doi.org/10.1002/0471721492.ch8.

[18] P. Quinn, M.S. Smith, J. Zhu, D.R.W. Hodgson, A.C. O'Donoghue, Triazolium Salt Organocatalysis: Mechanistic Evaluation of Unusual Ortho-Substituent Effects on Deprotonation, Catalysts 11 (2021) 1055. https://doi.org/10.3390/catal11091055.

[19] R.S. Massey, J. Murray, C.J. Collett, J. Zhu, A.D. Smith, A.C. O'Donoghue, Kinetic and structure–activity studies of the triazolium ion-catalysed benzoin condensation, Org. Biomol. Chem. 19 (2021) 387–393. https://doi.org/10.1039/D0OB02207A.

[20] Y. Niu, N. Wang, A. Muñoz, J. Xu, H. Zeng, T. Rovis, J.K. Lee, Experimental and Computational Gas Phase Acidities of Conjugate Acids of Triazolylidene Carbenes: Rationalizing Subtle Electronic Effects, J. Am. Chem. Soc. 139 (2017) 14917–14930. https://doi.org/10.1021/jacs.7b05229.

[21] J. Mahatthananchai, J.W. Bode, The effect of the N-mesityl group in NHC-catalyzed reactions, Chem. Sci. 3 (2012) 192–197. https://doi.org/10.1039/C1SC00397F.

[22] M. Pagacz-Kostrzewa, J. Krupa, W. Gul, M. Wierzejewska, FTIR matrix isolation studies of thermal decomposition of 1,2,4-triazolyl-3-carboxylic acid, Journal of Molecular Structure 1209 (2020) 127938. https://doi.org/10.1016/j.molstruc.2020.127938.

[23] B.P. Kar, W. Sander, Reversible Carbene Formation in the Ionic Liquid 1-Ethyl-3-Methylimidazolium Acetate by Vaporization and Condensation, ChemPhysChem 16 (2015) 3603–3606. https://doi.org/10.1002/cphc.201500729.

[24] O. Hollóczki, D. Gerhard, K. Massone, L. Szarvas, B. Németh, T. Veszprémi, L. Nyulászi, Carbenes in ionic liquids, New J. Chem. 34 (2010) 3004. https://doi.org/10.1039/c0nj00380h.

[25] Z. Kelemen, O. Hollóczki, J. Nagy, L. Nyulászi, An organocatalytic ionic liquid, Org. Biomol. Chem. 9 (2011) 5362. https://doi.org/10.1039/c1ob05639e.

[26] N. Akai, A. Kawai, K. Shibuya, Ion-Pair Structure of Vaporized Ionic Liquid Studied by Matrix-Isolation FTIR Spectroscopy with DFT Calculations: A Case of 1-Ethyl-3-

methylimidazolium Trifluoromethanesulfonate, J. Phys. Chem. A 114 (2010) 12662–12666. https://doi.org/10.1021/jp108209q.

[27] Williams, R. pKa Values in Water Compilation. ACS Division of Organic Chemistry, updated 4/7/2022. Available online: https://organicchemistrydata.org/hansreich/resources/pka/pka_data/pka-compilation-williams.pdf (accessed on 20 September 2024)., (n.d.).

[28] L.A. Daily, K.M. Miller, Correlating Structure with Thermal Properties for a Series of 1-Alkyl-4-methyl-1,2,4-triazolium Ionic Liquids, J. Org. Chem. 78 (2013) 4196–4201. https://doi.org/10.1021/jo4003932.

[29] A.D. Becke, Density-functional thermochemistry. III. The role of exact exchange, The Journal of Chemical Physics 98 (1993) 5648–5652. https://doi.org/10.1063/1.464913.

[30] C. Lee, W. Yang, R.G. Parr, Development of the Colle-Salvetti correlation-energy formula into a functional of the electron density, Phys. Rev. B 37 (1988) 785–789. https://doi.org/10.1103/PhysRevB.37.785.

[31] S.H. Vosko, L. Wilk, M. Nusair, Accurate spin-dependent electron liquid correlation energies for local spin density calculations: a critical analysis, Canadian Journal of Physics 58 (1980) 1200–1211. https://doi.org/10.1139/p80-159.

[32] M.J. Frisch, J.A. Pople, J.S. Binkley, Self-consistent molecular orbital methods 25. Supplementary functions for Gaussian basis sets, The Journal of Chemical Physics 80 (1984) 3265–3269. https://doi.org/10.1063/1.447079.

[33] P.J. Hay, W.R. Wadt, *Ab initio* effective core potentials for molecular calculations. Potentials for the transition metal atoms Sc to Hg, The Journal of Chemical Physics 82 (1985) 270–283. https://doi.org/10.1063/1.448799.

[34] S. Grimme, J. Antony, S. Ehrlich, H. Krieg, A consistent and accurate ab initio parametrization of density functional dispersion correction (DFT-D) for the 94 elements H-Pu, The Journal of Chemical Physics 132 (2010) 154104. https://doi.org/10.1063/1.3382344.

[35] M.J. Frisch, G.W. Trucks, H.B. Schlegel, G.E. Scuseria, M.A. Robb, J.R. Cheeseman, G. Scalmani, V. Barone, G.A. Petersson, H. Nakatsuji, X. Li, M. Caricato, A.V. Marenich, J. Bloino, B.G. Janesko, R. Gomperts, B. Mennucci, H.P. Hratchian, J.V. Ortiz, A.F. Izmaylov, J.L. Sonnenberg, D. Williams-Young, F. Ding, F. Lipparini, F. Egidi, J. Goings, B. Peng, A. Petrone, T. Henderson, D. Ranasinghe, V.G. Zakrzewski, J. Gao, N. Rega, G. Zheng, W. Liang, M. Hada, M. Ehara, K. Toyota, R. Fukuda, J. Hasegawa, M. Ishida, T. Nakajima, Y. Honda, O. Kitao, H. Nakai, T. Vreven, K. Throssell, J.A. Montgomery Jr., J.E. Peralta, F. Ogliaro, M.J. Bearpark, J.J. Heyd, E.N. Brothers, K.N. Kudin, V.N. Staroverov, T.A. Keith, R. Kobayashi, J. Normand, K. Raghavachari, A.P. Rendell, J.C. Burant, S.S. Iyengar, J. Tomasi, M. Cossi, J.M. Millam, M. Klene, C. Adamo, R. Cammi, J.W. Ochterski, R.L. Martin, K. Morokuma, O. Farkas, J.B. Foresman, D.J. Fox, Gaussian 16, Revision B.01, (2016).

[36] A.P. Thompson, H.M. Aktulga, R. Berger, D.S. Bolintineanu, W.M. Brown, P.S. Crozier, P.J. In 'T Veld, A. Kohlmeyer, S.G. Moore, T.D. Nguyen, R. Shan, M.J. Stevens, J. Tranchida, C. Trott, S.J. Plimpton, LAMMPS - a flexible simulation tool for particle-based

materials modeling at the atomic, meso, and continuum scales, Computer Physics Communications 271 (2022) 108171. https://doi.org/10.1016/j.cpc.2021.108171.

[37] T.D. Kühne, M. Iannuzzi, M. Del Ben, V.V. Rybkin, P. Seewald, F. Stein, T. Laino, R.Z. Khaliullin, O. Schütt, F. Schiffmann, D. Golze, J. Wilhelm, S. Chulkov, M.H. Bani-Hashemian, V. Weber, U. Borštnik, M. Taillefumier, A.S. Jakobovits, A. Lazzaro, H. Pabst, T. Müller, R. Schade, M. Guidon, S. Andermatt, N. Holmberg, G.K. Schenter, A. Hehn, A. Bussy, F. Belleflamme, G. Tabacchi, A. Glöß, M. Lass, I. Bethune, C.J. Mundy, C. Plessl, M. Watkins, J. VandeVondele, M. Krack, J. Hutter, CP2K: An electronic structure and molecular dynamics software package - Quickstep: Efficient and accurate electronic structure calculations, The Journal of Chemical Physics 152 (2020) 194103. https://doi.org/10.1063/5.0007045.

[38] L. Martínez, R. Andrade, E.G. Birgin, J.M. Martínez, P ACKMOL : A package for building initial configurations for molecular dynamics simulations, J Comput Chem 30 (2009) 2157–2164. https://doi.org/10.1002/jcc.21224.

[39] M. Thomas, M. Brehm, O. Hollóczki, Z. Kelemen, L. Nyulászi, T. Pasinszki, B. Kirchner, Simulating the vibrational spectra of ionic liquid systems: 1-Ethyl-3-methylimidazolium acetate and its mixtures, The Journal of Chemical Physics 141 (2014) 024510. https://doi.org/10.1063/1.4887082.

[40] S. Goedecker, M. Teter, J. Hutter, Separable dual-space Gaussian pseudopotentials, Phys. Rev. B 54 (1996) 1703–1710. https://doi.org/10.1103/PhysRevB.54.1703.

[41] M. Brehm, M. Thomas, S. Gehrke, B. Kirchner, TRAVIS—A free analyzer for trajectories from molecular simulation, The Journal of Chemical Physics 152 (2020) 164105. https://doi.org/10.1063/5.0005078.

[42] N.R. Dhumal, H.J. Kim, J. Kiefer, Molecular Interactions in 1-Ethyl-3-methylimidazolium Acetate Ion Pair: A Density Functional Study, J. Phys. Chem. A 113 (2009) 10397–10404. https://doi.org/10.1021/jp907394v.

[43] S.A. Katsyuba, E.E. Zvereva, A. Vidiš, P.J. Dyson, Application of Density Functional Theory and Vibrational Spectroscopy Toward the Rational Design of Ionic Liquids, J. Phys. Chem. A 111 (2007) 352–370. https://doi.org/10.1021/jp064610i.

[44] C. Maton, N. De Vos, C.V. Stevens, Ionic liquid thermal stabilities: decomposition mechanisms and analysis tools, Chem. Soc. Rev. 42 (2013) 5963. https://doi.org/10.1039/c3cs60071h.

[45] A. Engdahl, B. Nelander, Hydrogen iodide in argon matrixes, J. Phys. Chem. 90 (1986) 6118–6121. https://doi.org/10.1021/j100281a013.

[46] A.J. Barnes, H.E. Hallam, J.D.R. Howells, G.F. Scrimshaw, Infra-red cryogenic studies. Part 13.—Halogenoalkanes in argon matrices, J. Chem. Soc., Faraday Trans. 2 69 (1973) 738–749. https://doi.org/10.1039/F29736900738.

[47] F. Ito, T. Nakanaga, Y. Futami, S. Kudoh, M. Takayanagi, M. Nakata, Isomeric structures of CH3I dimers in a supersonic jet studied by matrix-isolation infrared

spectroscopy and ab initio calculation, Chemical Physics Letters 343 (2001) 185–191. https://doi.org/10.1016/S0009-2614(01)00688-1.

[48] A. Efimova, J. Varga, G. Matuschek, M.R. Saraji-Bozorgzad, T. Denner, R. Zimmermann, P. Schmidt, Thermal Resilience of Imidazolium-Based Ionic Liquids—Studies on Short- and Long-Term Thermal Stability and Decomposition Mechanism of 1-Alkyl-3-methylimidazolium Halides by Thermal Analysis and Single-Photon Ionization Time-of-Flight Mass Spectrometry, J. Phys. Chem. B 122 (2018) 8738–8749. https://doi.org/10.1021/acs.jpcb.8b06416.

[49] J.R. Cox, Stephen. Woodcock, I.H. Hillier, M.A. Vincent, Tautomerism of 1,2,3- and 1,2,4-triazole in the gas phase and in aqueous solution: a combined ab initio quantum mechanics and free energy perturbation study, J. Phys. Chem. 94 (1990) 5499–5501. https://doi.org/10.1021/j100377a016.

[50] M. Irvine, J. Mathieson, A. Pullin, The infrared matrix isolation spectra of carbon dioxide. II. Argon matrices: the CO2 monomer bands, Aust. J. Chem. 35 (1982) 1971. https://doi.org/10.1071/CH9821971.

[51] R.F.G. Apóstolo, G. Bazsó, R.R.F. Bento, G. Tarczay, R. Fausto, The first experimental observation of the higher-energy trans conformer of trifluoroacetic acid, Journal of Molecular Structure 1125 (2016) 288–295. https://doi.org/10.1016/j.molstruc.2016.06.077.

Declaration of interests

☒The authors declare that they have no known competing financial interests or personal relationships that could have appeared to influence the work reported in this paper.

☐The authors declare the following financial interests/personal relationships which may be considered as potential competing interests: